Stretchable light electrochemical cell based on $CsPbBr_3$ and distributed GaP nanowires array with single-walled carbon nanotubes electrode

Yakubova Anastasiya[a], Fedor Kochetkov[ab], Andrei S. Toikka[ab], Alexander Goltaev[a], Diana Kolesina[a], Dmitry M. Mitin[a], Eugene Malishev[a], Valeriy Kondratev[ac], Vladimir Fedorov[ad], Alexey D. Bolshakov[ace], Evgeniy Grigoryev[e], Dmitry Krasnikov[f], Albert G. Nasibulin[f], Sergey Makarov[bg], Ivan Mukhin[ad]*

[a] *Alferov University, Khlopina 8/3, 194021, St. Petersburg, Russia*
[b] *School of Physics and Engineering, ITMO University, Lomonosova 9, 197101, St. Petersburg, Russia*
[c] *Moscow Center for Advanced Studies, Kulakova str. 20, Moscow 123592*
[d] *Peter the Great St. Petersburg Polytechnic University, Polytechnicheskaya 29, 195251, St. Petersburg, Russia*
[e] *Saint-Petersburg State University, 7/9 Universitetskaya emb, 199034, St. Petersburg, Russia*
[f] *Kemerovo State University, Krasnaya Str. 6, Kemerovo, 650000, Russia*
[g] *Qingdao Innovation and Development Center, Harbin Engineering University, Qingdao, 266000, Shandong, China*

S1. Mathematical simulation of energy band diagrams for the n-GaP/CsPbBr

Numerical calculations were performed using Comsol Multiphysics in the drift-diffusion model approximation. The material parameters of GaP NWs and $CsPbBr_3$ were taken from[53,54]. The radiative recombination rate was calculated using van Roosbroeck–Shockley theory.

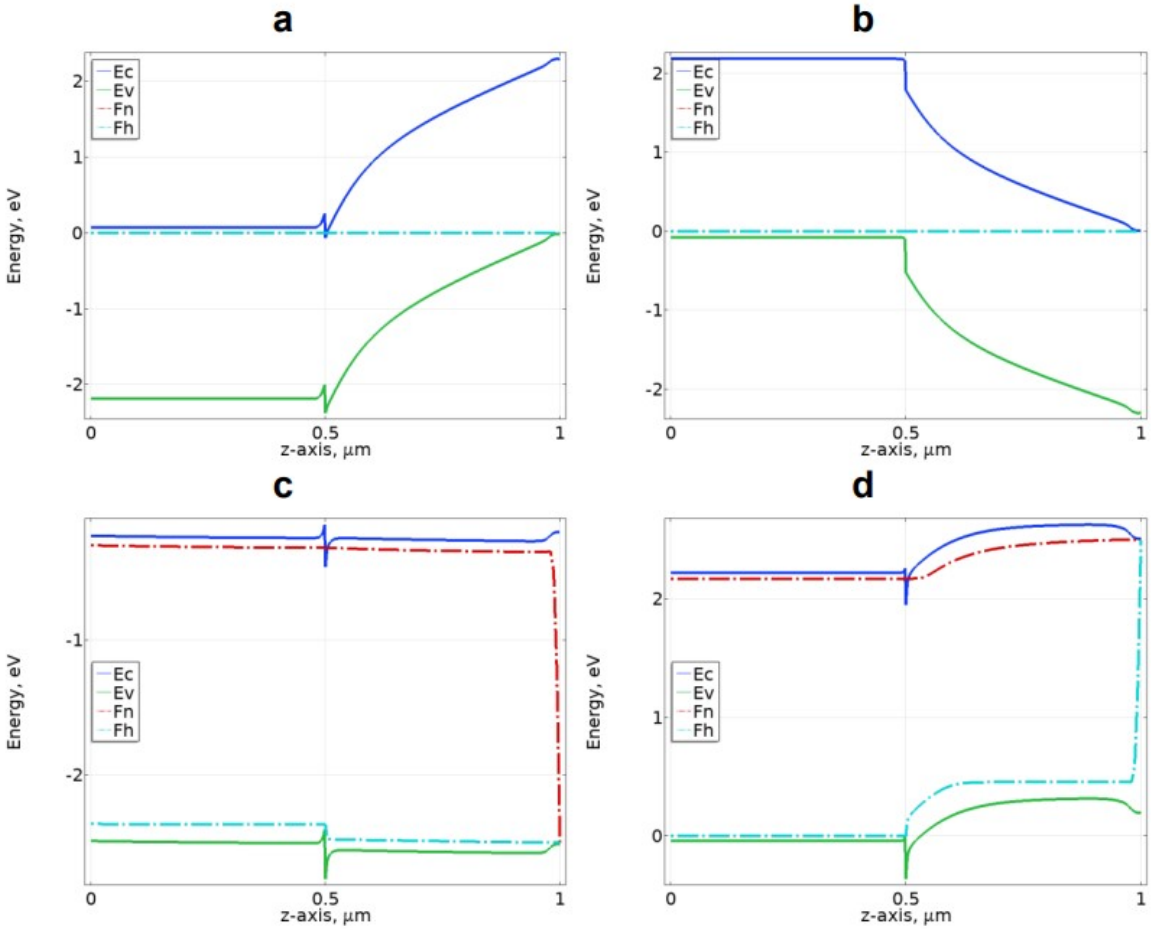

Figure S1. The calculated energy band diagrams for n-GaP/$CsPbBr_3$ (a, c) and p-GaP/$CsPbBr_3$ (b, d) heterojunctions, corresponding to an equilibrium state and 2.5 V external voltage. Ec, Ev, Fn, and Fh denote the conduction and valence bands, Fermi levels for electrons and holes, respectively.

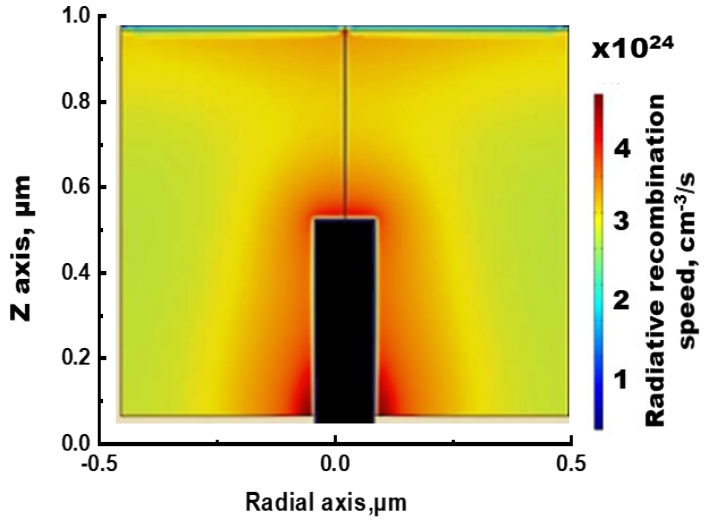

Figure S1.1. The calculated radiative recombination (reflecting the current distribution) near a single GaP NW (marked with a black rectangle), embedded into a $CsPbBr_3$ layer.

S2. Morphology of vertically-oriented GaP NWs.

Scanning electron microscopy (SEM) imaging of the grown and processed GaP NWs were performed using a Supra 25 (Carl Zeiss) microscope operated at (5-20) accelerating voltage. A typical SEM image of vertically-oriented GaP NWs grown on a Si substrate is shown in Figure S2.

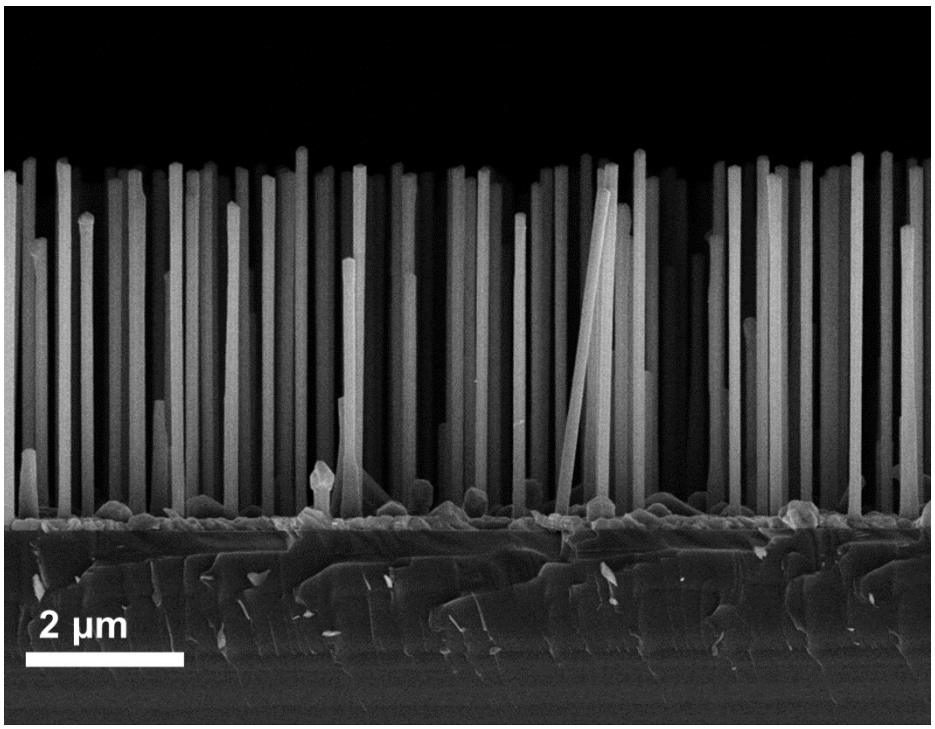

Figure S2. SEM image of vertically-grown n-doped GaP NWs on a Si substrate.

S3. XRD studies

X-ray diffraction (XRD) studies were performed on the functional PeLEC devices using a Bruker Kappa Apex II diffractometer equipped with a microfocus Incoatec IμS 1.0 Cu-Kα source (300 μm beam footprint) and a 2D charge-coupled detector. The perovskite samples were mounted with their surfaces normal to the diffractometer's phi-axis.

To analyze the possible formation of preferential orientation (crystal texture) in the perovskite films, three-dimensional reciprocal space maps (3D-RSMs) were collected by varying the angle of incidence (sample rocking along the omega axis). Despite the presence of the crystalline Si substrate and GaP NW array, no distinct texture was observed in all samples. The diffraction intensity was uniformly distributed along Debye-Scherrer rings, indicating an isotropic orientation of the perovskite crystallites. The only observed inhomogeneities resulted from the overlap of perovskite diffraction rings with intense reflections from the silicon substrate. For crystal phase analysis, diffraction patterns from the PeLEC samples were acquired at a fixed X-ray incidence angle of 12°. To enhance angular resolution, a series of overlapping 2D XRD images were collected at a large detector-to-sample distance of 180 mm, with the CCD detector fixed at 2Θ positions of 12, 20, 30, 40, 50, and 60°. Data was collected with a 20-min exposure time, while continuously rotating the sample about the phi-axis. The resulting 2D diffraction images were integrated using the DIOPTAS software[55] to obtain the one-dimensional diffraction profiles (2Θ curves) presented in Figure S3, covering a 2Θ range from 11 to 69.5°. The chosen

scattering geometry, with a relatively small detector solid angle of 0.116 sr, significantly reduced the chance to accidentally register an intense single-crystal diffraction from GaP NWs or Si substrate.

We observed only a small segment of the diffraction ring from the orthorhombic perovskite (122) and (212) planes ($2\Theta \approx 28.6°$) partially overlapped with the diffuse scattering arising from the intense GaP (111) ($2\Theta = 28.36°$) and Si (111) ($2\Theta = 28.47°$) reflections. These overlapping regions were masked and excluded during the integration process.

Both PeLEC samples (with different NW contact heights) exhibited an identical crystal structure, as evidenced by matching peak positions and full widths at half maximum in the XRD patterns (Figure S3). The detailed analysis confirmed that the observed XRD can be described by a single-phase orthorhombic $CsPbBr_3$ structure. The crystallographic information file (ID: 4510745) with lattice constants a = 8.244 Å, b = 8.198 Å, and c = 11.735 Å was adopted from the Crystallography Open Database (COD)[56]. The expected peak positions are marked by red rugs in Figure S3. The most intense reflexes from the high-symmetry planes are labeled on the XRD pattern. Notably, the diffraction curves contain no reflections associated with the formation of CsBr and $PbBr_2$ salts or other non-perovskite phases, indicating the stoichiometry of the perovskite precursors.

The only discernible difference between the samples is the intensity of the (002),(110) and (004),(220) reflections at 15.26° and 30.76°, respectively. Since the RSM analysis excluded preferential orientation in PeLEC samples, this variation is more likely to be attributed to the differences in scattering geometry, such as variations in the film thickness and morphology of the perovskite-NW composite.

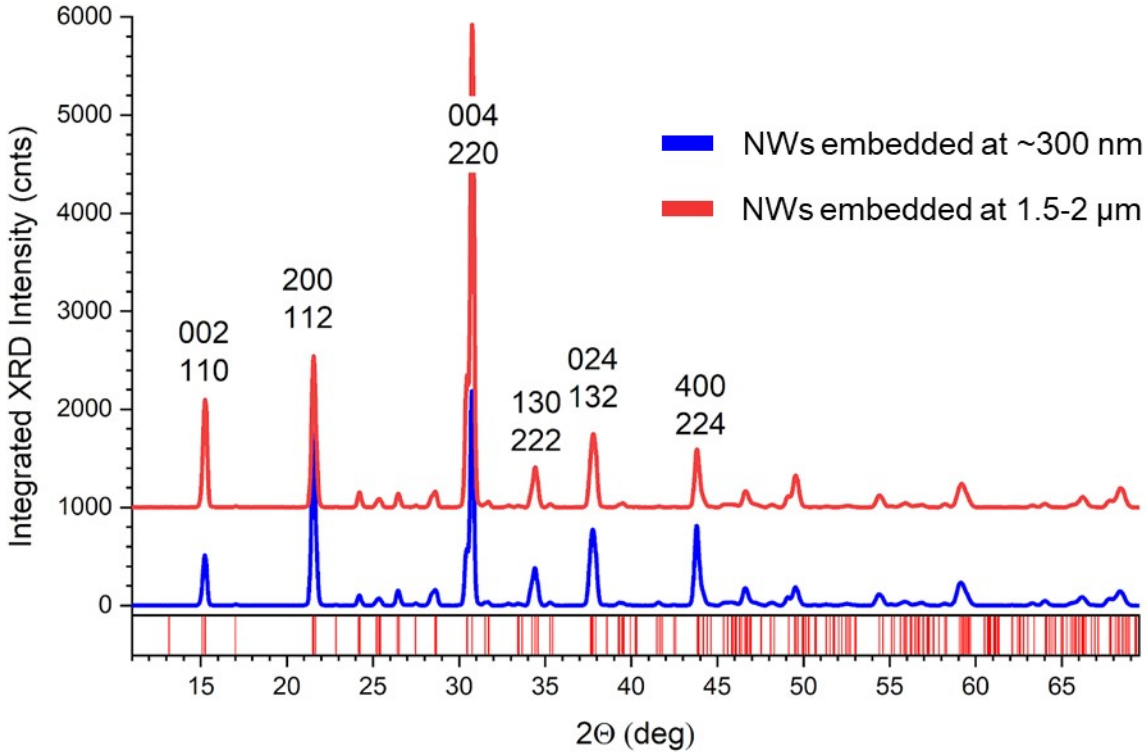

Figure S3. XRD of perovskite layers with different NWs contact heights of ~300 nm and 1.5-2µm (vertically offset for clarity).

S4. Emission color stability test under fixed 10% stretch

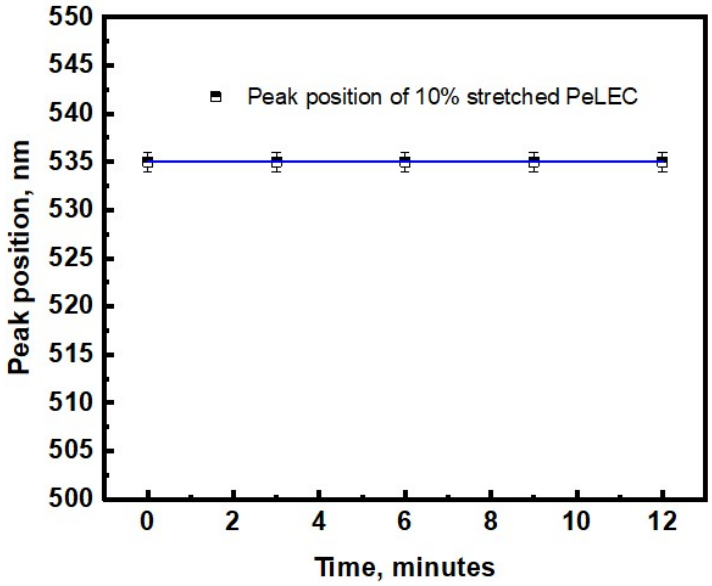

Figure S4. Emission color stability test under fixed 10% stretch.

S5. Stress-test machine

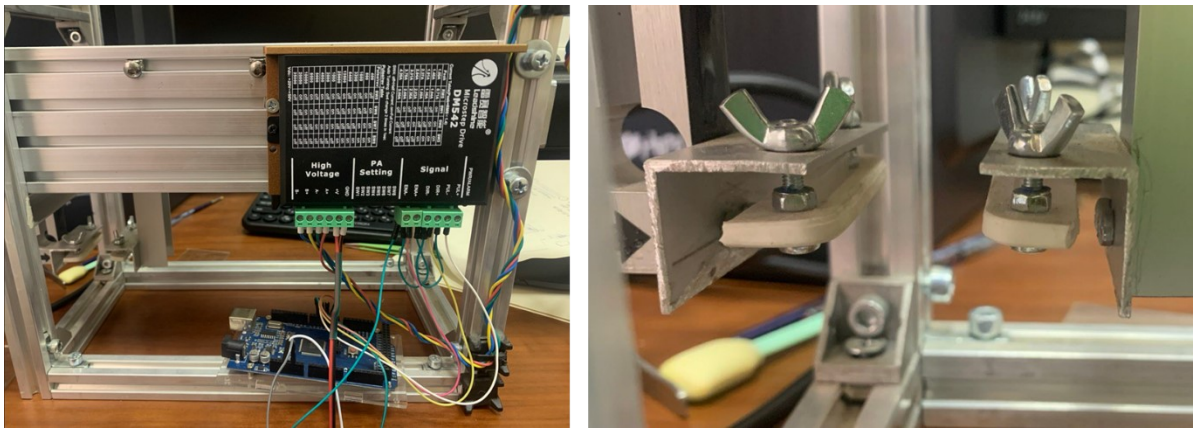

Figure S5. Stress-test machine with an accuracy of stretching of 10 μm: overview - left panel, clamping mechanism - right panel.

S6. Stress test analysis

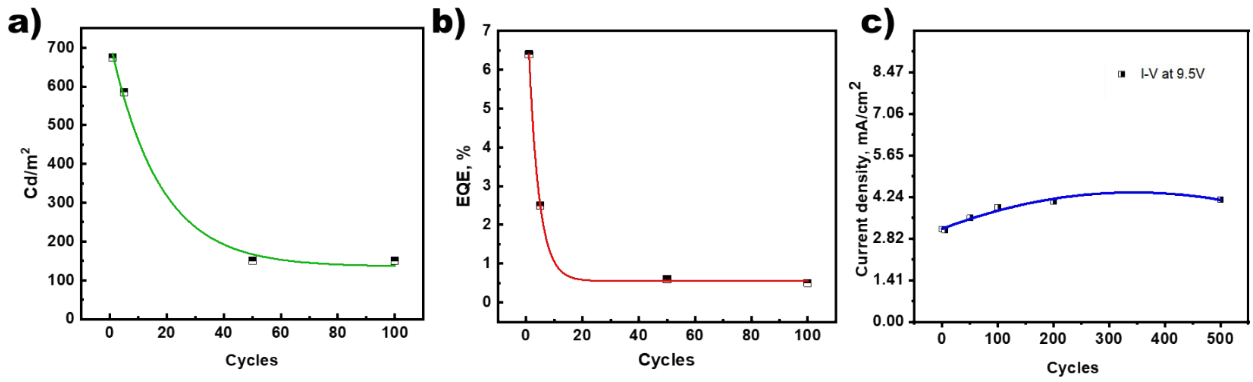

Figure S6. Dependencies of (a) luminance and (b) EQE on stretching/relaxation cycles, c) current density on stretching/relaxation cycles.